DOI: 10.1002/cmdc.200800410

Structure-Based Optimization of Aldose Reductase Inhibitors Originating from Virtual Screening

Michael Eisenmann, Holger Steuber, Matthias Zentgraf, Mirko Altenkämper, Regina Ortmann, Johann Perruchon, Gerhard Klebe,* and Martin Schlitzer*[a]

Diabetes mellitus is a universal health problem. The World Health Organization (WHO) estimates that 150 million people suffer from diabetes mellitus worldwide in 2005. Long-term complications are a serious problem in the treatment of diabetes, manifesting in macrovascular and microvascular complications. Sorbitol accumulation has been proposed to be an important factor in the development of microvascular complications such as nephropathy, neuropathy, retinopathy or cataract. Catalyzing the NADPH-dependent reduction of glucose to sorbitol, aldose reductase (ALR2) is an important target in the prevention of these complications. The development of novel aldose reductase inhibitors is expected to benefit strongly from a structure-based design approach. A virtual screening based on the ultrahigh-resolution crystal structure of the inhibitor IDD 594 in complex with human ALR2 identified two compounds with IC_{50} values in the low micro- to submicromolar range. Based on the known interactions between the ligands and their binding pocket, we simplified the lead structures to give the minimal structural requirements and developed synthetic pathways from commercially available compounds. The newly synthesized compounds were assayed for their inhibition of ALR2, showing inhibitory activities down to the nanomolar range. Crystal structure analysis of the most potent derivative of our series revealed insights into the binding mode of the inhibitors.

Introduction

Diabetes mellitus is a universal health problem. The World Health Organization (WHO) estimates that the present number of 150 million people suffering from diabetes worldwide will double by the year 2025. Prior to the introduction of insulin in the diabetic therapy in 1921, ~60% of the patients died of coma caused by acidosis.[1] Today, at least in the well-developed countries, the expected mean life span has been successfully increased. Better control of hyperglycemia was achieved through new forms of insulin and insulin delivery,[2] newer therapeutic modalities (e.g. intensified insulin treatment)[3,4] and recommendations for improved prevention (e.g. medical nutrition therapy, physical activity).[5]

Even though the blood-glucose level can be better controlled, it is still impossible to completely prevent the occurrence of hyperglycemic events. Therefore, the problems and challenges in diabetic therapy are increasingly shifted. Diabetes patients suffer from long-term complications, manifested in macrovascular and microvascular complications. Prevalence at diagnosis for microvascular complications are: neuropathy (9%), retinopathy (20%) and overt diabetes nephropathy ($\leq$10%),[6,7] limiting the patients life quality tremendously. Moreover, approximately four million deaths worldwide are related to diabetes mellitus, caused primarily by cardiovascular complications, representing the main macrovascular complications.

The new challenge in the treatment of diabetes is to further improve the glycemic control and to prevent long-term complications. A well-known major contribution to various long-term complications is the sorbitol pathway (also known as the polyol pathway). Aldose reductase catalyzes the first step of the polyol pathway, reducing glucose to sorbitol, using NADPH as a cofactor. Due to the comparably low affinity of glucose to ALR2 under normoglycemia, most of the glucose is phosphorylated by hexokinase and only a small proportion of glucose enters the polyol pathway. Under hyperglycemia the flux through the polyol pathway increases to one third of the total glucose turnover,[8,9] leading to significant sorbitol accumulation in cells that take up glucose in an insulin-independent manner. This may cause tissue damage by an increasing intracellular osmolarity, previously recognized as a main cause of long-term complications.[10,11] In more recent studies, other polyol pathway-related metabolic alterations rather than sorbitol accumulation were focused on, such as myo-inositol depletion, increased oxidative stress, glycation or altered protein kinase C activity.[12,13,14] As enhanced aldose reductase activity has been shown to be involved in several of these imbalances, it is a promising target for preventing long-term complications of diabetes.

While a broad variety of compounds have been synthesized or extracted from natural sources over the past few decades, only a few drug candidates have reached clinical trials. Epalre-

[a] M. Eisenmann, H. Steuber, M. Zentgraf, M. Altenkämper, R. Ortmann, J. Perruchon, G. Klebe, M. Schlitzer
Institut für Pharmazeutische Chemie, Philipps Universität Marburg
Marbacher Weg 6, 35032 Marburg (Germany)
Fax: (+49) 642-128-8994
E-mail: klebe@mailer.uni-marburg.de

Supporting information for this article is available on the WWW under http://dx.doi.org/10.1002/cmdc.200800410.

 © 2009 Wiley-VCH Verlag GmbH & Co. KGaA, Weinheim

stat (Kinedak®) is the only available inhibitor on the market (Japan), used to treat diabetic peripheral neuropathy, whereas Tolrestat came to market but was withdrawn in 1996 due to its suspected toxicity. However, some agents are in clinical trials (Zenarestat,[15] Zopolrestat, phase III; Minalrestat, AS-3201, Japan, phase II, many others are in phase I clinical trials[16,17]). With the potential benefit of aldose reductase inhibitors in diabetes long-term complications, renewed efforts promise the design of novel and efficient compounds.

The plethora of well-resolved crystal structures of aldose reductase predestines this enzyme as a promising target for rational drug design. Human aldose reductase is a 36 kD TIM-barrel-shaped aldo-keto reductase,[18] operating on a wide range of structurally diverse substrates due to pronounced induced fit adaptations.[19] Analyzing the various ALR2 crystal structures reveals more details about the ALR2 binding pocket, which is divided by Trp 111 into the catalytic subpocket and the specificity pocket. The catalytic subpocket is deeply buried, composed of residues presumably involved in the catalytic mechanism (Tyr 48, Lys 77, His 110). Additionally, the nicotinamide moiety of $NADP^+$ and Trp 111 interact with the head group of most described ligands. Hydrophobic contacts can be formed by the side chains of Trp 20, Val 47, Trp 79, and Trp 219. This catalytic subpocket is usually addressed by hydrophilic, negatively charged anchor groups. Ligands decorated at one end by appropriate hydrophobic groups induce, to varying extend, the opening of distinct pockets referred to as specificity pocket conformers. These pockets are formed by Ala 299, Leu 300 and Phe 122 at the solvent-exposed face and the side chain of Trp 111 oriented towards the center of the TIM barrel.[20,21,22,23]

Diffraction data of ALR2 in complex with the potent inhibitor IDD 594 have been measured and refined to a resolution of 0.66 Å. The crystal structure provides evidence for the protonation states of the titratable and catalytically relevant residues involved in inhibitor binding.[24] Based on this crystal structure with experimentally assigned protonation states, a virtual screening study has been performed. This screening resulted in six new carboxylate-type lead compounds. Two of these showed affinities in the low micro- to submicromolar range (**1**: $IC_{50}=0.53$ μM, **2**: $IC_{50}=4.1$ μM).[25,26]

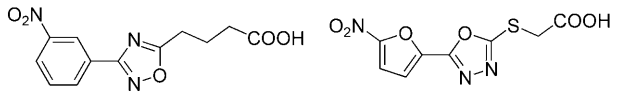

1 **2**

Recently, the crystal structures of these ligands in complex with ALR2 were determined in our laboratory.[26] Both ligands contain a nitro-substituted terminal moiety linked to a 5-membered heterocycle connected via an alkyl spacer to the carboxylic head group (Figure 1).

These characteristic features were used to create a first pharmacophore model (Figure 2): a carboxylic anchor group should occupy the anionic binding pocket, whereas, linked to this head group via an alkyl spacer, a lipophilic biaryl moiety should induce the opening of the specificity pocket between Trp 111 and Leu 300.

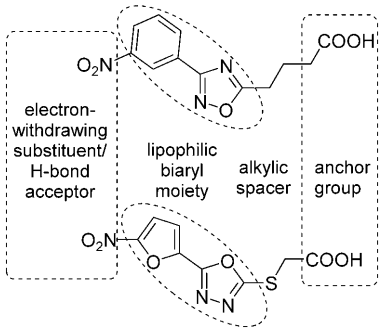

Figure 1. Structural features of compounds **1** and **2**.

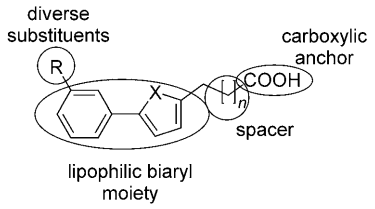

Figure 2. Basic pharmacophore model.

As demonstrated by crystal structure analysis, several heteroatoms present in compounds **1** and **2** are not involved in direct polar interactions with binding site residues. These atoms are present without particular purpose, as these compounds were not designed to bind to ALR2, but discovered as hits by virtual screening from a large sample of commercially available compounds. Polar ligand atoms that remain unsatisfied by corresponding counter groups in the protein will most have a strong influence on an imbalanced polar contact inventory. To avoid such effects that could be detrimental to high affinity binding, the original screening hits should profit from a removal of the heteroatoms not involved in binding. For this reason we designed and synthesized furan and thiophene derivatives instead of the oxadiazole moiety present in the original lead structures.

Finally, we established a synthesis for 3-(5-phenylfuran-2-yl)-propanoic acid derivatives and the corresponding thiophene derivatives. Furthermore, the 4-oxo-butanoic acids as well as butanoic acids were prepared in good yields, starting from commercially available compounds. Further modeling studies with the ALR2–**1** crystal structure led to the synthesis of 3-(2-phenylthiazol-5-yl)propanoic acid regioisomers and 3-(5-pyridylfuran-2-yl)propanoic acid regioisomers.

Results and Discussion

Chemical synthesis

Scheme 1 illustrates the synthesis of phenylfurylpropanoic acids **7** and phenylthiophenepropanoic acids **8**. Suzuki coupling in aqueous solution with varying phenylboronic acid derivatives and bromofurane carbaldehyde or bromothiophene

 © 2009 Wiley-VCH Verlag GmbH & Co. KGaA, Weinheim

These are not the final page numbers!

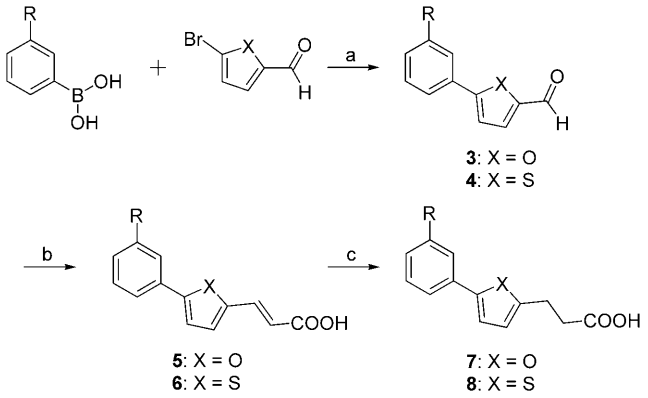

Scheme 1. Synthesis of phenylfurylpropanoic acids **7** and phenylthiophenepropanoic acids **8**. *Reagents and conditions*: a) K_2CO_3, $(Bu)_4NBr$, $Pd(OAc)_2$, H_2O/acetone, RT; b) malonic acid, pyridine/piperidine, reflux; c) Pd/$SrCO_3$ or Pd/C, H_2, MeOH/EtOAc, RT.

carbaldehyde, respectively, catalyzed by palladium acetate provided the diverse biarylic aldehyde precursors **3** and **4**. Knoevenagel condensation with malonic acid in pyridine with catalytic amounts of piperidine (Doebner modification) converted them into the *E*-acrylic acids **5** and **6**. Reduction of the double bond by hydrogenation with palladium on charcoal (thiophene derivatives) or palladium on strontium carbonate (furan derivatives) yielded the propanoic acids **7** and **8** as final compounds. The 3-amino derivative **7e** was prepared by hydrogenation of the 3-nitro compound **5h**.

For the synthesis of the pyridine derivatives **7i** and **7j** Suzuki coupling was carried out with the bromopyridine derivative and 5-formylfuran-2-boronic acid in a mixture of 1,2-dimethoxyethane and aqueous sodium carbonate solution with $PdCl_2$(dppf) and $Pd(PPh_3)_4$ as catalysts. The following steps were carried out as described above.

Nitro derivatives, sensitive to hydrogenation, were prepared by reduction of the corresponding biarylic carbaldehyde **3h** and **4h** with sodium borohydride to the corresponding alcohol **9** and **10**, respectively. Treatment with thionyl chloride afforded the chloromethyl derivative, which was reacted with diethylmalonate to yield **11** and **12**, respectively. Acid-catalyzed ester hydrolysis and decarboxylation furnished the acids **7h** and **8h** (Scheme 2).

Compound **13** was synthesized by cyclization of thiobenzamide with 2-chloromalonedialdehyde in acetone. Synthesis of compound **16** started from thiobenzamide and 1,3-dichloroacetone, resulting in the chloromethyl derivative. Finkelstein reaction led to the iodomethyl compound, followed by treatment with urotropine and paraformaldehyde yielding the carbaldehyde **16**.

Knoevenagel condensation and hydrogenation yielded the propanoic acids **15** (Scheme 3) and **18** (Scheme 4).

Scheme 5 describes the synthesis of 4-oxo-butanoic acids **20a** and **20b** and butanoic acids **21a** and **21b**. As described above, the biaryl precursors were prepared by Suzuki coupling. Subsequent Friedel–Crafts acylation provided the 4-oxo derivatives. Finally, Wolf–Kishner reduction resulted in the butanoic acids.

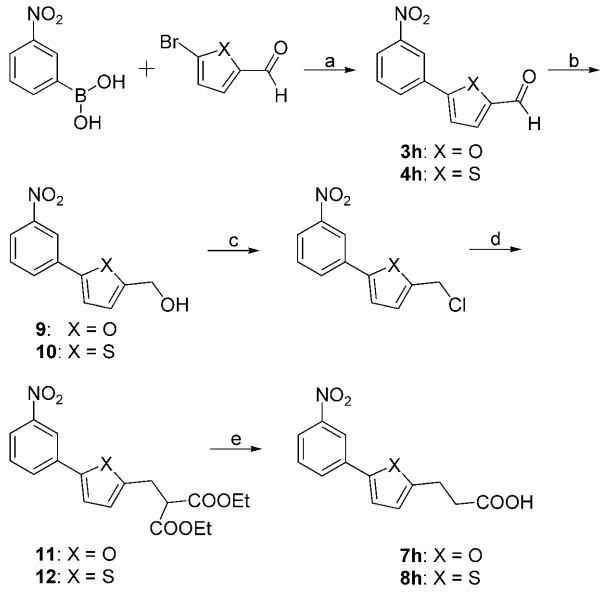

Scheme 2. Synthesis of nitro substituted propanoic acids **7h** and **8h**. *Reagents and conditions*: a) K_2CO_3, $(Bu)_4NBr$, $Pd(OAc)_2$, H_2O or H_2O/acetone, RT; b) $NaBH_4$, THF, 4 h, RT; c) $SOCl_2$, CH_2Cl_2, RT; d) diethylmalonate, NaH, RT; e) 6 M HCl, reflux.

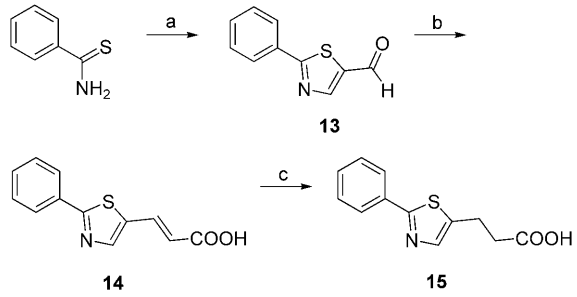

Scheme 3. Synthesis of thiazol-5-yl derivative **15**. *Reagents and conditions*: a) 2-chloromalone dialdehyde, acetone, reflux; b) malonic acid, pyridine/piperidine, reflux; c) Pd/charcoal, H_2, MeOH/EtOAc, RT.

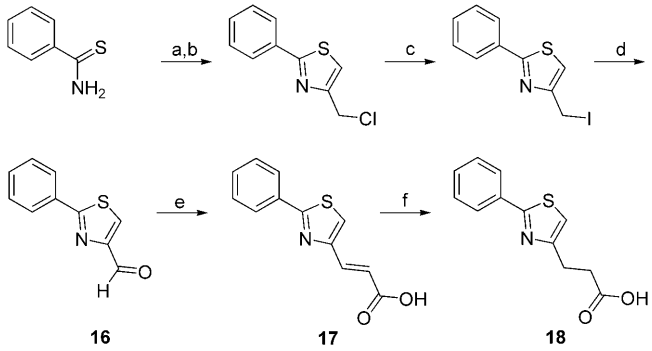

Scheme 4. Synthesis of thiazol-4-yl derivative **18**. *Reagents and conditions*: a) 1,3-dichloroacetone, acetone, RT; b) H_2SO_4, RT; c) KI, EtOH/H_2O, reflux; d) urotropine, paraformaldehyde, 50% AcOH, reflux; e) malonic acid, pyridine/piperidine, reflux; f) Pd/charcoal, H_2, MeOH/EtOAc, RT.

 © 2009 Wiley-VCH Verlag GmbH & Co. KGaA, Weinheim

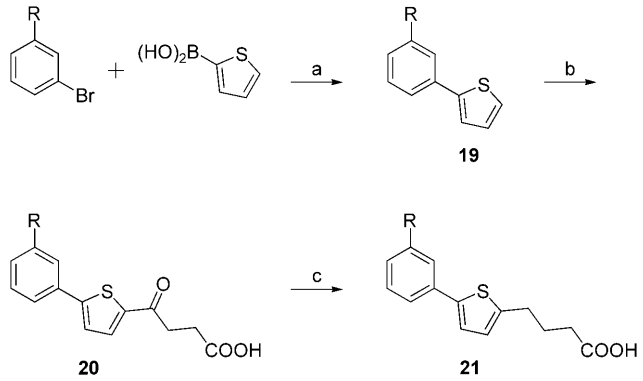

Scheme 5. Synthesis of 4-oxo butanoic acids **20** and butanoic acids **21**. *Reagents and conditions*: a) K_2CO_3, $(Bu)_4NBr$, $Pd(OAc)_2$, H_2O or H_2O/acetone, RT; b) succinic anhydride, dichloroethane, $AlCl_3$; $-5\,^{\circ}C \rightarrow RT$; c) KOH, $NH_2NH_2 \cdot H_2O$, diethylene glycol, 180 °C.

Binding pocket

Crystal structure determination of compounds **1** and **2** in complex with ALR2 provided insights into the binding geometry of both lead compounds. In summary, the carboxylate groups of both compounds **1** and **2** occupy the catalytic pocket of the enzyme, whereas the aromatic portion induces the opening of the specificity pocket located between Trp 111 and Leu 300. Unexpectedly, the slightly longer alkyl spacer of **1**, compared with **2**, enables the carboxylate to occupy the catalytic pocket with a deviating interaction geometry compared to the one known from other structures; whereas carboxylate-type inhibitors usually directly interact with Tyr 48 OH, His 110 NE2 and Trp 111 NE1, in the ALR2–**1** complex the latter contact is mediated via an interstitial water molecule. This water molecule is not observed in the ALR2–**2** complex, while the overall binding characteristics of **2** are maintained. Based on this crystallographic analysis and evaluation of the affinity data collected for compounds **1** and **2** we embarked on a synthesis program to systematically vary the ligand composition and to thereby identify structure–activity relationships.

Biological evaluation and structure–activity relationship

All compounds were tested for their inhibition of ALR2. Inhibition constants were determined using an absorbance assay based on the fact that ALR2 catalyzes the reduction of aldehydes using NADPH with an accompanying decrease in absorbance at 340 nm. The results of the biological evaluation are given in Table 1.

To identify preliminary structure–activity relationships, we replaced all polar core atoms not involved in binding to the protein (unless they were required for synthetic reasons) leading to the propionic acid derivatives **7a** and **8a** (Table 1), as well as to the butyric acid-type ligand **21a** (Table 2). Interestingly, despite most of the heteroatoms having been replaced and the nitro substituent omitted, all three derivatives exhibit a similar affinity as observed for compound **2**. This underlines the hypothesis that the presence of these polar components does not contribute significantly to the binding affinity. In addition, these three derivatives allow the influence of the alkyl spacer length to be studied. Assuming similar binding geometries for the compounds **1** and **21a**, as well as for compounds **2** and **7a**, **8a**, the affinity data suggest no evidence for a bene-

Table 1. Inhibition of ALR2.

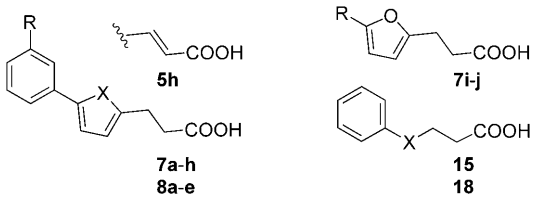

Compound	R	X	IC_{50}[a] [μM]
5h	NO_2	O	19 ± 0.9
7a	H	O	16 ± 1.5
8a	H	S	5.3 ± 0.8
7b	CH_3	O	5.7 ± 0.9
8b	CH_3	S	4.9 ± 0.7
7c	OCH_3	O	6.8 ± 1.5
8c	OCH_3	S	5.4 ± 0.9
7d	CF_3	O	2.0 ± 0.27
8d	CF_3	S	1.9 ± 0.23
7h	NO_2	O	0.26 ± 0.05
8h	NO_2	S	0.17 ± 0.03
7f	$COCH_3$	O	3.0 ± 0.5
7g	SO_2CH_3	O	4.0 ± 1.4
7e	NH_2	O	16 ± 3.6
7i		–	19 ± 2.9
7j		–	31 ± 3.8
15	–		14 ± 2.1
18	–	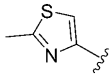	22 ± 3.9

Measurements were carried out at least in duplicate.

Table 2. Inhibition of ALR2.

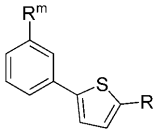

R = 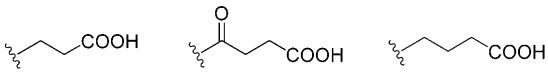

R^m	Cmpd	IC_{50}[a] [μM]	Cmpd	IC_{50}[a] [μM]	Cmpd	IC_{50}[a] [μM]
H	**8a**	5.3 ± 0.8	**20a**	6.5 ± 1.9	**21a**	6.4 ± 1.8
CH_3	**8b**	4.9 ± 0.7	**20b**	4.1 ± 0.7	**21b**	3.1 ± 0.6

Measurements were carried out at least in duplicate.

 © 2009 Wiley-VCH Verlag GmbH & Co. KGaA, Weinheim

These are not the final page numbers!

ficial contribution to binding affinity in case of the extended alkyl chain. Variations of the substitution pattern have been performed in the *meta* position of the terminal aromatic moiety, as the ALR2–**1** and ALR2–**2** complexes suggested, there is sufficient space available to accommodate additional small substituents. Similarly to **7a**, **8a** and **21a**, a related trend is observed for the methyl-substituted series **7b**, **8b**, **21b** and the methoxy-substituted compounds **7c** and **8c**. Obviously, the methoxy group originally introduced in order to address putative H-bond donors within the specificity pocket (such as Thr 113 OG or Leu 300 NH) does not lead to a significant improvement in affinity. In order to evaluate whether the putative beneficial character of such an H-bond acceptor might be superseded by a detrimental contribution caused by decreasing the strength of the π–π stacking between the Trp 111 indole moiety and the aromatic tail of the ligand when electron-donating groups are present, we replaced the methoxy group with acetyl and methylsulfonyl substituents (**7f**, **7g**). Both derivatives only exhibit a marginal improvement in affinity compared to **7a-c** and **8a-c**, respectively, possibly provoked by increasing the π–π interactions upon introduction of electron-withdrawing groups in the aromatic tail. Consistently, introduction of even more electron-donating groups such as an amino function in **7e** leads to an unchanged or even poorer affinity compared to compounds **7a** and **8a**. These results prompted us to introduce a trifluoromethyl substituent with even more electron-withdrawing properties at the corresponding position resulting in ~2 μM affinity (**7d** and **8d**). The ALR2–**1** complex suggested that the nitro group is involved in an H bond to Leu 300 NH, and nonclassical polar interactions with the aromatic CH groups of Tyr 309. As the nitro group combines electron-withdrawing properties likely to enhance the stacking interaction with the efficient formation of polar contacts, the introduction of a nitro group, as present in the lead structures, appeared promising. Indeed, both nitro-substituted derivatives **7h** and **8h**, containing either a furan or thiophene nucleus, exhibit a higher affinity than the more potent lead compound **1**. Remarkably, immobilization of the alkyl spacer by introduction of an *E* double bond (**5h**) parallels a loss in affinity by approximately two orders of magnitude.

This provokes the question of whether replacement of the substituted phenyl moiety by an electron deficient bioisosteric system will enhance affinity. Two pyridine derivatives were synthesized (**7i**, **7j**) but both exhibit a decrease in affinity of at least two orders of magnitude. Thus, the pyridine moiety is obviously not able to mimic the interactions established by the nitro phenyl portion in a comparable manner. A further optimization strategy is based on addressing the Leu 300 backbone NH group with appropriate acceptors, as successfully demonstrated by the enhanced affinity of fidarestat compared to sorbinil. We attempted to achieve this interaction by the appropriate incorporation of a nitrogen atom into the scaffold of **8b** leading to the derivatives **15** and **18**. Similarly, as observed in the complexes ALR2–**1** and ALR2–**2**, where the heteroatoms of the five-membered aromatic ring are too remote to efficiently form H bonds, also for the two synthesized derivatives, no improvement of affinity was observed.

Crystal structure analysis

In order to determine whether the performed optimization was accompanied by a change in binding mode with respect to the target, we determined the crystal structure of aldose reductase in complex with derivative **8h**.

As expected, the overall binding geometry is maintained for **8h** and corresponds to that of **2** (Figure 3). The carboxylate head occupies the catalytic pocket, whereas the hydrophobic

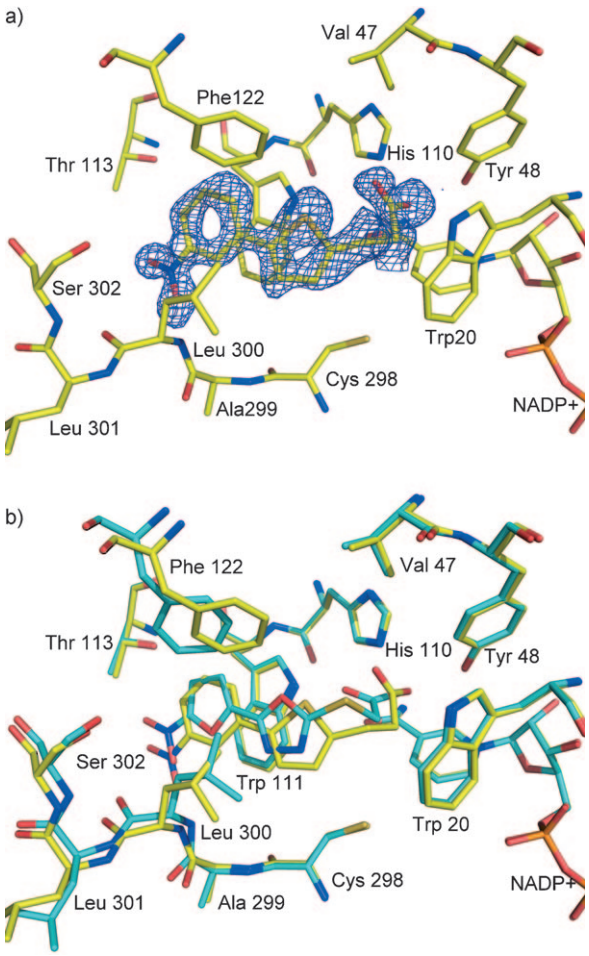

Figure 3. Crystal structure analysis of compound **8h**: a) Binding geometry of **8h** in the ALR2 binding pocket at 1.45 Å. The 2Fo–Fc electron density at 1.5 σ is shown in blue; b) Superposition of the complex structures observed for **2** (cyan) and **8h** (yellow).

tail is located within the specificity pocket. The nonclassical polar interactions between the nitro group and the aromatic side chain of Tyr 309 seem to be stronger in the case of **8h** compared with **2** as suggested by shorter distances between donor and acceptor atoms. Unexpectedly, in ALR2–**8h**, the carboxylate head group adopts a kinked conformation compared to ALR2–**2**, where the ligand carboxylate is oriented coplanar with respect to the nicotinamide moiety of the cofactor. The orientation observed in ALR2–**8h** prevents the formation of a polar contact between the carboxylate and the Trp 111 NE1 donor group, whereas the H bonds to Tyr 48 OH and His 110

 © 2009 Wiley-VCH Verlag GmbH & Co. KGaA, Weinheim

NE2 are established as observed in ALR2–**2**. The origin of this deviating geometry is difficult to explain. Putatively, the larger van der Waals radius of the sulfur atom in **8h** compared with the oxygen atom in compound **2** prevents a similar orientation of the carboxylate. If no further compensating adaptations are in operation, the carboxylate oxygen expected to interact with Trp 111 NE1 would have to approach the sulfur atom at a distance as close as 2.2 Å in order to adopt an identical position. As this appears to be an unfavorably short contact, it might explain the observed deviating positioning of the carboxylate anchor in ALR2–**8h**.

Conclusions

Due to the lack of optimal properties in aldose reductase inhibitors presently in clinical trials, the search for novel potent ligands is of utmost importance. In our study, two similar lead compounds with slightly deviating affinities were identified by virtual screening. In drug development projects, the decision to select the most promising candidate for further optimization from a series of various putative leads is difficult, as the final success of such a process largely depends on the most appropriate choice of a development candidate. In a previous study, we performed a structural characterization of our two leads via X-ray crystallography.[26] This study suggested the replacement of several heteroatoms in the core skeleton that are not involved in polar interactions with the binding site residues as a putative strategy for lead optimization. Obviously, in the present case these heteroatoms influence the solvation/desolvation properties unfavorably. Following this strategy, we developed efficient synthetic routes to obtain a series of ALR2 inhibitors. These ligands are derivatives of the original virtual screening hits, however, they comprise reduced complexity and therefore allow for a better understanding of the structure–activity relationships with respect to the parent inhibitor scaffold. Admittedly, some of our optimization concepts failed and resulted in partially comparable or even lower inhibitory potency compared to the original leads. This might be caused by the fact that the expected interactions, which guided our design strategy, were not formed or were compensated for by other effects. The series of derivatives confirms our results from a previous study[26] emphasizing the significant contribution of the nitro group to binding affinity. The present study provides deeper insights into the structure–activity relationships and thereby paves the way for further structure-guided design efforts.

Experimental Section

Biology

Enzymatic inhibition assay: The in vitro inhibitory activities of the candidate molecules were determined by recording the decrease in NADPH absorbance upon enzymatic reduction of xylitol. The absorbance at 340 nm was monitored at 25 °C with a BMG plate reader. The assay was performed using a polypropylene plate with 250 μL of reaction mixture: sodium phosphate buffer (100 mM, pH 6.2) containing NADPH (0.14 mM), D-xylose as substrate (26.5 mM) and human ALR2 (0.28 μM). Test compounds were assayed for inhibition at concentrations ranging from 0.8–20 nM. The program GraFit75 (Version 4.0)[27] was used for fitting the IC_{50} values. All kinetic measurements were carried out at least in duplicate. Given inhibition data and standard deviations have been obtained from data fitting and subsequent averaging.

Enzyme purification and crystallization: Cloning, expression, purification and crystallization of ALR2 have already been described elsewhere.[20–26] Prior to crystallization, ALR2 solutions were concentrated to 20 mg mL^{-1} in 50 mM diammonium hydrogen citrate at pH 5 and mixed with a solution of the cofactor in an oxidized state to achieve a molar ratio of ALR2:$NADP^+$ of 1:3. ALR2–inhibitor complexes were obtained by cocrystallization with **8h** (5 mM) in the protein solution. After an equilibration period of one week, microseeding was performed. Crystals were grown at 293 K using the hanging drop vapor diffusion method. Crystals were usually obtained one to two days after microseeding.

Data collection: Data were collected at 100 K using a cryoprotectant solution of 40% (*m/v*) PEG 6000 in 50 mM diammonium hydrogen citrate at pH 5. The data sets were collected on a RIGAKU copper rotating anode (Molecular Structure Cooperation) at 50 kV, 90 mA using a R-AXIS IV++ image plate system. For each frame, the exposure time and oscillation range were set to 5 min and 0.5°, respectively. Data processing and scaling were performed using the HKL2000 package.[28]

Structure determination and refinement

The coordinates of human ALR2 (PDB code 1L3) were used for initial rigid-body refinement of the protein atoms followed by repeated cycles of conjugate gradient energy minimization, simulated annealing and B-factor refinement using the CNS program package.[29] Refinement at later stages was performed with the program SHELXL.[30] Here, at least 20 cycles of conjugate gradient minimization were performed with default restraints on bonding geometry and B-values. Of all data, 5% was used for R_{free} calculation. Amino acid side chains were fitted into sigma A-weighted $2F_o$–F_c and F_o–F_c electron density maps using the program O.[31] After the first refinement cycle, water molecules and subsequently cofactor and ligand were located in the electron density and added to the model. Restraints were applied to bond lengths and angles, chiral volume, planarity of aromatic rings and van der Waals contacts. Multiple side-chain conformations were built in case an appropriate electron density was observed and maintained during the refinement, and if the minor populated side chain showed at least 10% occupancy. During the last refinement cycle, riding H atoms were introduced without using additional parameters. The final models were validated using PROCHECK.[32] Data collection, unit cell parameters and refinement statistics are given in the Supporting Information. Figures were prepared using Isis Draw (MDL, San Leandro, USA) and Pymol.[33] The coordinates of the ALR2–**8h** complex have been deposited in the Protein Data Bank under the PDB code 3DN5.

Chemistry

NMR spectra were recorded on a Jeol Eclipse Plus instrument (^{1}H NMR: 500 MHz or 400 MHz, chemical shifts (δ) are reported in ppm relative to the central residual solvent peak. Coupling constants (J) are given in Hz. For purification purposes, flash column chromatography (FC) was performed using silica gel (particle size 0.040–0.063 mm) supplied by Merck. Analytical thin-layer chroma-

 © 2009 Wiley-VCH Verlag GmbH & Co. KGaA, Weinheim

These are not the final page numbers!

tography (TLC) was carried out on Merck silica gel 60 F254 plates. High resolution mass spectra (EI) were performed with a JMS-GCmate II spectrometer. Elemental analyses for C, H, and N are within 0.4% of the calculated values and were performed on an Elementar Vario EL.

5-Phenyl-furan-2-carbaldehyde (**3a**), 5-(3-methoxyphenyl)furan-2-carbaldehyde (**3c**), 5-(3-methoxyphenyl)thiophene-2-carbaldehyde (**4c**), 5-phenylthiophene-2-carbaldehyde (**4a**) were synthesized as described by Bussolari and co-workers.[34] 2-Phenythiazole-5-carbaldehyde (**13**) and 2-phenylthiazole-4-carbaldehyde (**16**) were synthesized as described by Silberg.[35,36] 5-(3-Nitrophenyl)furan-2-carbaldehyde (**3h**) and 5-phenylthiophene (**19a**) were obtained from Acros Organics. (*E*)-3-(5-Phenylfuran-2-yl)acrylic acid (**5a**), (*E*)-3-(5-(3-trifluormethyl)phenylfuran-2-yl)acrylic acid (**5d**), (*E*)-3-(5-(3-nitrophenyl)furan-2-yl)acrylic acid (**5h**) were synthesized as described by Mitsch et al. carried out in our group.[37,38]

*General procedure 1: Preparation of biarylic carbaldehydes (**3/4**) via Suzuki coupling.*

5-Bromofuran-2-carbaldehyde (1.0–1.4 equiv), the phenyl boronic acid component (1.0 equiv), $(Bu)_4NBr$ (1.0 equiv), K_2CO_3 (2.5 equiv) and $Pd(OAc)_2$ (5 mg mmol^{-1}, minimum of 20 mg) were dissolved/suspended in H_2O and vigorously stirred for 2 h. Acetone was added and the reaction was stirred further stirred for 1 h. The reaction mixture was diluted with H_2O and extracted with EtOAc (×2). The combined organic phases were stirred with charcoal (~1 g mmol^{-1} of bromo component) and Na_2SO_4 for 30 min and evaporated after filtration. The residue was purified by flash chromatography.

5-(3-Methylphenyl)furan-2-carbaldehyde (**3b**): orange solid, yield: 87%. FC: silica gel, *n*-hexane/EtOAc 4:1. ^{1}H NMR ($CDCl_3$, 500 MHz): δ = 2.41 (s, 3H), 6.82 (m, 1H), 7.20–7.21 (m, 1H), 7.30–7.34 (m, 2H), 7.60–7.62 (m, 1H), 7.65–7.66 (m, 1H), 9.4 (s, 1H).

5-(3-Trifluormethylphenyl)furan-2-carbaldehyde (**3d**): orange solid, yield: 74%. FC: silica gel, *n*-hexane/EtOAc 4:1. ^{1}H NMR ($CDCl_3$, 500 MHz): δ = 6.93 (m, 1H), 7.34 (m, 1H), 7.57 (m, 1H), 7.64 (m, 1H), 7.99 (m, 1H), 8.04 (s, 1H), 9.68 ppm (s, 1H).

5-(3-Acetylphenyl)furan-2-carbaldehyde (**3f**): pale orange solid, yield: 63%. FC: silica gel, *n*-hexane/EtOAc 4:1. ^{1}H NMR ($CDCl_3$, 500 MHz): δ = 2.67 (s, 3H), 6.94 (m, 1H), 7.34 (m, 1H), 7.56 (m, 1H), 7.96–7.98 (m, 1H), 8.01–8.03 (m, 1H), 8.36–8.37 (m, 1H), 9.69 ppm (s, 1H).

5-(3-Methylsulfonylphenyl)furan-2-carbaldehyde (**3g**): orange solid, yield: 92%. FC: silica gel, EtOAc/isohexane 3:2. ^{1}H NMR ($CDCl_3$, 400 MHz): δ = 3.11 (s, 3H), 6.98 (m, 1H), 7.35 (m, 1H), 7.67 (m, 1H), 7.95 (m, 1H), 8.10 (m, 1H), 8.34 (m, 1H), 9.70 ppm (s, 1H).

5-(3-Methylphenyl)thiophene-2-carbaldehyde (**4b**): brown-orange solid, yield: 95%. ^{1}H NMR ($CDCl_3$, 500 MHz): δ = 2.41 (s, 3H), 7.20 (m, 1H), 7.31 (m, 1H), 7.38 (m, 1H, 7.45–7.49 (m, 2H), 7.73 (m, 1H), 9.88 ppm (s, 1H).

5-(3-(Trifluormethyl)phenyl)thiophene-2-carbaldehyde (**4d**): pale orange solid, yield: 53%, FC: silica gel, *n*-hexane/EtOAc 4:1. ^{1}H NMR ($CDCl_3$, 400 MHz): δ = 7.46 (m, 1H), 7.56 (m, 1H), 7.64 (m, 1H), 7.70 (m, 1H), 7.83 (m, 1H), 7.89 (m, 1H), 9.91 ppm (s, 1H).

5-(3-Nitrophenyl)thiophene-2-carbaldehyde (**4h**): orange solid, yield: 18%, FC: silica gel, *n*-hexane/EtOAc 7:3. ^{1}H NMR ($CDCl_3$, 500 MHz): δ = 7.54 (m, 1H), 7.64 (m, 1H), 7.80 (m, 1H), 7.98 (m, 1H), 8.25 (m, 1H), 8.53 (m, 1H), 9.94 ppm (s, 1H).

5-(Pyridine-2-yl)furan-2-carbaldehyde (**3i**): ochre solid, yield: 44%. ^{1}H NMR ($CDCl_3$, 500 MHz): δ = 7.25 (m, 1H), 7.28 (m, 1H), 7.35 (m, 1H), 7.78 (m, 1H), 7.92 (m, 1H), 8.65 (m, 1H), 9.71 ppm (s, 1H). ^{13}C NMR ($CDCl_3$, 125 MHz): δ = 110.7, 120.1, 123.0, 123.9, 137.0, 147.9, 150.0, 152.7, 158.4, 177.7 ppm.

5-(Pyridine-3-yl)furan-2-carbaldehyde (**3j**): ochre solid, yield: 65%. ^{1}H NMR ($CDCl_3$, 500 MHz): δ = 6.95–6.97 (m, 1H), 7.34–7.35 (m, 1H), 7.42–7.45 (m, 1H), 8.16 (m, 1H), 8.62–8.63 (m, 1H), 9.06 (s, 1H), 9.70 ppm (s, 1H). ^{13}C NMR ($CDCl_3$, 100 MHz) δ = 108.7, 123.1, 123.8, 125.2, 132.2, 146.6, 150.3, 152.6, 156.3, 177.4 ppm.

*General procedure 2: Formation of biarylacrylic acids (**5/6**) via Knoevenagel condensation.*

The aromatic aldehyde was dissolved in a mixture of pyridine (5 mL) and piperidine (0.2 mL). After addition of malonic acid (125 mg per mmol ofaldehyde), the mixture was heated under reflux for 2 h. After cooling, this mixture was poured into a mixture of H_2O (60 mL), ice (60 mL), and concd HCL (60 mL) to yield a solid that was filtered and washed with *n*-pentane. In the case of compounds **5i** and **5j** the mixture was not poured into HCl; the solvent was removed into a liquid nitrogen cooled receiving flask. The residue was washed with *n*-pentane and Et_2O, dissolved in a minimum amount of EtOAc and precipitated with *n*-pentane.

(*E*)-3-(5-Phenyl-furan-2-yl)acrylic acid (**5a**): *orange solid,* yield: 83%. ^{1}H NMR ([D$_6$]DMSO, 500 MHz): δ = 6.33 (d, *J* = 15.7 Hz, 1H), 7.03 (m, 1H), 7.13 (m, 1H), 7.36 (m, 1H), 7.42 (d, *J* = 15.7 Hz, 1H), 7.44–7.48 (m, 2H,), 7.81–7.85 (m, 2H′), 12.39 ppm (s, 1H). ^{13}C NMR ([D$_6$]DMSO, 125 MHz): δ = 108.7, 115.9, 117.9, 124.1, 128.5, 129.0, 129.4, 130.5, 150.0, 155.2, 167.4 ppm. HRMS (EI): calcd for $C_{13}H_{10}O_3$: 214.0630; found: 214.0636.

(*E*)-3-(5-(3-Methylphenyl)furan-2-yl)acrylic acid (**5b**): orange solid, yield: 76%. ^{1}H NMR (Acetone-d$_6$, 400 MHz): δ = 2.38 (s, 3H), 6.40 (d, *J* = 15.6 Hz, 1H), 6.94 (m, 1H), 7.00 (m, 1H), 7.16–7.20 (m, 1H), 7.33 (m, 1H), 7.48 (d, *J* = 15.6 Hz, 1H), 7.63–7.67 (m, 1H), 7.68–7.71 (m, 1H), 10.80 ppm (s, 1H). ^{13}C NMR (Acetone-d$_6$, 100 MHz): δ = 21.4, 108.9, 115.9, 118.5, 122.3, 125.6, 129.7, 130.1, 130.7, 131.8, 139.4, 151.1, 157.0, 167.8 ppm. HRMS (EI): calcd for $C_{14}H_{12}O_3$: 228.0787; found: 228.0798.

(*E*)-3-(5-(3-Methoxyphenyl)furan-2-yl)acrylic acid (**5c**): ochre solid, yield: 77%. ^{1}H NMR (Acetone-d$_6$, 500 MHz): δ = 3.86 (s, 3H), 6.41 (d, *J* = 15.7 Hz, 1H), 6.92 (m, 1H), 6.95 (m, 1H), 7.03 (m, 1H), 7.36 (m, 1H), 7.39 (m, 1H), 7.41–7.45 (m, 1H), 7.48 ppm (d, *J* = 15.7 Hz, 1H). ^{13}C NMR (Acetone-d$_6$, 100 MHz): δ = 55.7, 109.3, 110.3, 115.2, 116.2, 117.6, 118.4, 130.9, 131.8, 132.0, 151.3, 156.7, 161.2, 167.8 ppm. HRMS (EI): calcd for $C_{14}H_{12}O_4$: 244.0736; found: 244.0727.

(*E*)-3-(5-(3-(Trifluormethyl)phenyl)furan-2-yl)acrylic acid (**5d**): orange solid, yield: 47%. ^{1}H NMR (Acetone-d$_6$, 400 MHz): δ = 6.49 (d, *J* = 15.8 Hz, 1H), 7.03 (m, 1H), 7.25 (m, 1H), 7.51 (d, *J* = 15.8 Hz, 1H), 7.68–7.72 (m, 2H), 8.14–8.19 (m, 2H), 10.90 ppm (s, 1H). ^{13}C NMR ([D$_6$]DMSO, 125 MHz) δ = 109.6, 116.1, 117.0, 119.7 (q, J_{C-F} = 3.8), 123.2 (q, J_{C-F} = 272.1), 123.9 (q, J_{C-F} = 3.8), 127.1, 129.2 (q, J_{C-F} = 31.7), 129.41, 129.49, 129.54, 149.9, 152.6, 166.6 ppm. ^{19}F NMR (Acetone-d$_6$, 470 MHz): δ = −61.10 ppm. HRMS (EI): calcd for $C_{14}H_9F_3O_3$: 282.0504; found: 282.0459.

(*E*)-3-(5-(3-Acetylphenyl)furan-2-yl)acrylic acid (**5f**): red-brownish solid, yield: 68%. ^{1}H NMR (Acetone-d$_6$, 400 MHz): δ = 2.66 (s, 3H), 6.46 (d, *J* = 15.8 Hz, 1H), 7.00 (m, 1H), 7.18 (m, 1H), 7.51 (d, *J* = 15.7 Hz, 1H) 7.61 (m, 1H), 7.96 (m, 1H 1H), 8.10 (m, 1H), 8.40 ppm (m, 1H). ^{13}C NMR (Acetone-d$_6$, 100 MHz): δ = 26.8, 110.0, 116.6, 118.4, 124.6, 128.8, 129.2, 130.2, 131.2, 131.7, 138.9, 151.7, 155.8,

 © 2009 Wiley-VCH Verlag GmbH & Co. KGaA, Weinheim

167.7, 197.7 ppm. EI-HRMS: calcd for $C_{15}H_{12}O_4$: 256.0736; found: 256.0734.

(*E*)-3-(5-(3-(Methylsulfonyl)phenyl)furan-2-yl)acrylic acid (**5g**): yellow solid, yield: 55%. ^{1}H NMR ([D$_6$]DMSO, 500 MHz): δ=3.31 (s, 3H), 6.42 (d, J=15.9 Hz), 7.08 (m, 1H), 7.34 (m, 1H), 7.44 (d, J=15.9 Hz, 1H), 7.73 (m, 1H), 7.88 (m, 1H), 8.17 (m, 1H), 8.30 ppm (m, 1H). ^{13}C NMR ([D$_6$]DMSO, 125 MHz): δ=43.3, 110.5, 117.0, 117.9, 122.1, 126.3, 128.8, 130.26, 130.29, 130.4, 141.9, 150.8, 153.2, 167.3 ppm. HRMS (EI): calcd for $C_{14}H_{12}O_5S$: 292.0405; found: 292.0423.

(*E*)-3-(5-(3-Nitrophenyl)furan-2-yl)acrylic acid (**5h**): yellow-orange solid, yield: 63%. ^{1}H NMR ([D$_6$]DMSO, 400 MHz): δ=6.45 (d, J=15.9 Hz, 1H), 7.11 (m, 1H), 7.44 (m, 1H), 7.45 (d, J=15.7 Hz, 1H), 7.76 (m, 1H), 8.18–8.21 (m, 1H), 8.28–8.31 (m, 1H), 8.59 (m, 1H), 12.50 ppm (b, 1H). ^{13}C NMR ([D$_6$]DMSO, 100 MHz): δ=111.0, 117.2, 117.8, 118.3, 122.7, 130.1, 130.2, 130.7, 130.9, 148.5, 151.0, 152.6, 167.2 ppm. HRMS (EI): calcd for $C_{13}H_9NO_5$: 259.048; found: 259.0467.

(*E*)-3-(5-(Pyridine-2-yl)furan-2-yl)acrylic acid (**5i**): orange solid, yield: 87%. ^{1}H NMR ([D$_6$]DMSO, 400 MHz) δ=6.41 (d, J=15.7 Hz, 1H), 6.95 (m, 1H), 7.20 (m, 1H), 7.27 (d, J=15.7 Hz, 1H), 7.31–7.35 (m, 1H), 7.85–7.91 (m, 2H), 8.59–8.62 ppm (m, 1H). ^{13}C NMR ([D$_6$]DMSO, 125 MHz): δ_C (ppm)=111.2, 116.5, 119.0, 119.8, 123.0, 128.8, 137.3, 147.8, 149.8, 151.5, 154.3, 168.1 ppm. HRMS (EI): calcd for $C_{12}H_9NO_3$: 215.0582 found: 215.0581.

(*E*)-3-(5-(Pyridine-3-yl)furan-2-yl)acrylic acid (**5j**): ochre solid, yield: 80%. ^{1}H NMR ([D$_6$]DMSO, 500 MHz): δ=6.38 (d, J=15.8 Hz, 1H), 6.84 (m, 1H), 7.14 (d, J=15.8 Hz, 1H), 7.21 (m, 1H), 7.45–7.48 (m, 1H), 8.14 (m, 1H), 8.51 (m, 1H), 9.01 ppm (m, 1H). ^{13}C NMR ([D$_6$]DMSO, 125 MHz) δ_C (ppm)=109.8, 115.6, 121.8, 124.0, 125.7, 127.4, 130.9, 145.2, 148.8, 151.5, 151.7, 168.8 ppm. HRMS (EI): calcd for $C_{12}H_9NO_3$: 215.0582; found: 215.0577.

(*E*)-3-(5-Phenylthiophene-2-yl)acrylic acid (**6a**): yellowish solid, yield: 86%. ^{1}H NMR ([D$_6$]DMSO, 500 MHz): δ=6.18 (d, J=15.7 Hz, 1H), 7.36 (m, 1H), 7.45 (m, 2H), 7.53 (m, 1H), 7.57 (m, 1H), 7.69–7.71 (m, 2H), 7.73 ppm (d, J=15.9 Hz, 1H). ^{13}C NMR ([D$_6$]DMSO, 125 MHz) δ=117.3, 124.9, 125.6, 128.5, 129.2, 133.0, 133.3, 136.6, 138.1, 146.1, 167.2 ppm. HRMS (EI): calcd for $C_{13}H_{10}O_2S$: 230.0402; found: 230.0390.

(*E*)-3-(5-(3-Methylphenyl)thiophene-2-yl)acrylic acid (**6b**): ochre solid, yield: 98%. ^{1}H NMR ([D$_6$]DMSO, 500 MHz): δ=2.35 (s, 3H), 6.17 (d, J=15.7 Hz, 1H), 7.18 (m, 1H), 7.33 (m, 1H), 7.49–7.54 (m, 4H), 7.73 (d, J=15.7 Hz, 1H), 12.40 ppm (s, 1H). ^{13}C NMR ([D$_6$]DMSO, 125 MHz) δ=21.0, 117.3, 122.8, 124.8, 126.1, 129.2, 129.3, 133.0, 133.4, 136.8, 138.0, 138.6, 146.4, 167.3 ppm. HRMS (EI): calcd for $C_{14}H_{12}O_2S$: 244.0558; found: 244.0508.

(*E*)-3-(5-(3-Methoxyphenyl)thiophene-2-yl)acrylic acid (**6c**): red-brownish solid, yield: 95%. ^{1}H NMR (Acetone-d$_6$, 400 MHz): δ=3.86 (s, 3H), 6.24 (d, J=15.6 Hz, 1H), 6.94 (m, 1H), 7.24–7.30 (m, 2H), 7.35 (m, 1H), 7.45 (m, 1H), 7.50 (m, 1H), 7.79 ppm (d, J=15.6 Hz, 1H). ^{13}C NMR (Acetone-d$_6$, 100 MHz) δ=55.7, 112.0, 114.9, 117.5, 119.0, 125.6, 131.1, 133.8, 135.7, 138.0, 139.5, 147.7, 161.2, 166.5 ppm. HRMS (EI): calcd for $C_{14}H_{12}O_3S$: 260.0507; found: 260.0533.

(*E*)-3-(5-(3-(Trifluormethyl)phenyl)thiophene-2-yl)acrylic acid (**6d**): orange solid, yield: 83%. ^{1}H NMR (Acetone-d$_6$, 400 MHz): δ=6.29 (d, J=15.6 Hz, 1H) 7.51–7.53 (m, 1H), 7.67–7.71 (m, 3H), 7.81 (dd, J_1=15.6 Hz, J_2=0.7 Hz, 1H), 7.98–8.03 ppm (m, 2H). ^{13}C NMR (Acetone-d$_6$, 100 MHz): δ=118.3, 123.0, 123.4 (q, J_{C-F}=271.5 Hz), 125.7, 126.8, 130.4, 131.2, 131.8 (q, J_{C-F}=31.5 Hz) 133.8, 135.5, 137.8, 140.7, 145.5, 167.3 ppm. HRMS (EI): calcd for $C_{14}H_9F_3O_2S$: 298.0275; found: 298.0280.

(*E*)-3-(2-Phenylthiazole-5-yl)acrylic acid (**14**): pale yellow solid, yield: 70%. ^{1}H NMR ([D$_6$]DMSO, 500 MHz): δ=6.26 (d, J=15.8 Hz, 1H), 7.52–7.56 (m, 3H), 7.84 (d, J=15.8 Hz, 1H), 7.96 −7.99 (m, 2H), 8.26 (s, 1H), 12.55 ppm (s, 1H). ^{13}C NMR ([D$_6$]DMSO, 100 MHz): δ=120.9, 126.5, 129.4, 131.1, 132.6, 133.7, 134.7, 147.7, 166.9, 168.7 ppm. HRMS (EI): calcd for $C_{12}H_9NO_2S$: 231.0354; found: 231.0339.

(*E*)-3-(2-Phenylthiazole-4-yl)acrylic acid (**17**): white solid, yield: 97%. ^{1}H NMR ([D$_6$]DMSO, 500 MHz): δ=6.67 (s, J=15.7 Hz, 1H), 7.52–7.55 (m, 3H), 7.61 (d, J=15.7 Hz, 1H), 7.98–8.02 (m, 2H), 8.13 (s, 1H), 12.50 ppm (s, 1H). ^{13}C NMR ([D$_6$]DMSO, 100 MHz) δ=120.9, 123.6, 126.4, 129.3, 130.8, 132.5, 136.2, 151.9, 167.5, 167.8 ppm. HRMS (EI): calcd for $C_{12}H_9NO_2S$: 231.0345; found: 231.0341.

*General procedure 3: Preparation of biaryl propanoic acids (**7/8**) via catalytic hydrogenation.*

The biarylic precursor was dissolved in a mixture of MeOH and EtOAc (10–20 mL, various ratios depending on solubility). The hydrogenation was carried out under a 1 atm pressure of H_2 at RT. The progress of the reaction was followed by the consumption of H_2. After the hydrogenation was completed the reaction was filtered through a mixture of silica gel and celite, followed by evaporation and purification by flash chromatography with silica gel.

3-(5-Phenylfuran-2-yl)propanoic acid (**7a**): pale yellow solid, yield: 51%. FC: silica gel, CH_2Cl_2/MeOH 95:5. ^{1}H NMR ($CDCl_3$, 400 MHz): δ=2.78 (t, J=7.7 Hz, 2H), 3.04 (t, J=7.7 Hz, 2H), 6.12 (m, 1H), 6.54 (m, 1H), 7.22 (m, 1H), 7.33–7.37 (m, 2H), 7.60–7.62 ppm (m, 2H). ^{13}C NMR ([D$_6$]DMSO, 100 MHz): δ=23.3, 32.5, 105.7, 107.7, 123.4, 127.0, 128.6, 130.9, 152.8, 153.4, 178.7 ppm. HRMS (EI): calcd for $C_{13}H_{12}O_3$: 216.0787; found: 216.0789.

3-(5-(3-Methylphenyl)furan-2-yl)propanoic acid (**7b**): white solid, yield: 29%. FC: silica gel, CH_2Cl_2/MeOH 95:5. ^{1}H NMR ([D$_6$]DMSO, 400 MHz): δ=2.33 (s, 3H), 2.62 (t, J=7.5 Hz, 2H), 2.91 (t, J=7.5 Hz, 2H), 6.21 (m, 1H), 6.79 (m, 1H), 7.05–7.08 (m, 1H), 7.28 (m, 1H), 7.42–7.48 ppm (m, 2H). ^{13}C NMR ([D$_6$]DMSO, 100 MHz): δ=21.0, 23.1, 31.9, 106.3, 107.4, 120.2, 123.3, 127.6, 128.6, 130.3, 137.9, 151.5, 154.2, 173.4 ppm. HRMS (EI): calcd for $C_{14}H_{14}O_3$: 230.0943; found: 230.0947.

3-(5-(3-Methoxyphenyl)furan-2-yl)propanoic acid (**7c**): pale orange solid, yield: 69%. FC: silica gel, CH_2Cl_2/MeOH 9:1. ^{1}H NMR ([D$_6$]DMSO, 400 MHz): δ=2.78 (t, J=7.7 Hz, 2H), 3.05 (t, J=7.7 Hz, 2H), 3.85 (s, 3H), 6.13 (m, 1H), 6.54 (m, 1H), 6.75–6.81 (m, 1H), 7.15–7.18 (m, 1H), 7.19–7.23 (m, 1H), 7.27 ppm (m, 1H). ^{13}C NMR ([D$_6$]DMSO, 100 MHz): δ=23.2, 32.0, 55.1, 106.9, 107.6, 108.3, 112.7, 115.5, 130.0, 131.8, 151.3, 154.5, 159.6, 173.5 ppm. HRMS (EI): calcd for $C_{14}H_{14}O_4$: 246.0892; found: 246.0891.

3-(5-(3-Trifluormethyl)phenylfuran-2-yl)propanoic acid (**7d**): orange solid, yield: 40%. FC: silica gel, CH_2Cl_2/MeOH 9:1. ^{1}H NMR ($CDCl_3$, 400 MHz): δ=2.79 (t, J=7.7 Hz, 2H), 3.05 (t, J=7.7 Hz, 2H), 6.16 (m, 1H), 6.63 (m, 1H), 7.45–7.47 (m, 2H), 7.75–7.79 (m, 1H), 7.84 ppm (m, 1H). ^{13}C NMR ($CDCl_3$, 100 MHz): δ=23.3, 32.3, 107.1, 108.0, 120.1 (q, J_{C-F}=3.8 Hz), 123.4 (q, J_{C-F}=3.8 Hz), 124.1 (q, J_{C-F}=272.5 Hz), 126.4 (q, J_{C-F}=1.5 Hz), 129.1, 131.1 (q, J_{C-F}=32.2 Hz), 131.5, 151.3, 154.3, 177.9 ppm. HRMS (EI): calcd for $C_{14}H_{11}F_3O_3$: 284.0660; found: 284.0660.

3-(5-(3-Aminophenyl)furan-2-yl)propanoic acid (**7e**): orange solid, yield: 62%. FC: silica gel, CH_2Cl_2/MeOH 92:8. ^{1}H NMR ([D$_6$]DMSO,

 © 2009 Wiley-VCH Verlag GmbH & Co. KGaA, Weinheim

These are not the final page numbers!

500 MHz): $\delta = 2.58$ (t, $J = 7.7$ Hz, 2H), 2.88 (t, $J = 7.7$ Hz, 2H), 5.10 (s, 2H), 6.17 (m, 1H), 6.45 (m, 1H), 6.60 (m, 1H), 6.78–6.81, (m, 1H), 6.86 (m, 1H), 7.02 ppm (m, 1H). ^{13}C NMR ([D$_6$]DMSO, 100 MHz): $\delta =$ 23.5, 32.7, 105.5, 107.2, 108.3, 111.1, 112.9, 129.2, 131.0, 148.9, 152.2, 154.2, 174.1 ppm. HRMS (EI): calcd for $C_{13}H_{13}NO_6$: 231.0895; found: 231.0916.

3-(5-(3-Acetylphenyl)furan-2-yl)propanoic acid (**7f**): pale yellow solid, yield: 52%. FC: silica gel, CH_2Cl_2/MeOH 9:1. ^{1}H NMR ($CDCl_3$, 500 MHz): $\delta = 2.64$ (s, 3H), 2.78 (t, $J = 7.7$ Hz, 2H), 3.06 (t, $J = 7.7$ Hz, 2H), 6.16 (m, 1H), 6.63 (m, 1H), 7.45 (m, 1H), 7.79 (m, 2H), 8.18 ppm (m, 1H). ^{13}C NMR ($CDCl_3$, 100 MHz): $\delta = 23.3$, 26.7, 32.3, 106.7, 107.9, 123.1, 126.8, 127.8, 128.9, 131.4, 137.5, 151.7, 154.1, 177.8, 198.1 ppm. HRMS (EI): calcd for $C_{15}H_{14}O_4$: 258.0892; found: 258.0879.

3-(5-(3-Methylsulfonyl)phenylfuran-2-yl)propanoic acid (**7g**): orange solid, yield: 42%. ^{1}H NMR (Acetone-d$_6$, 400 MHz): $\delta = 2.74$ (t, $J =$ 7.7 Hz, 2H), 3.04 (t, $J = 7.7$ Hz, 2H), 3.16 (s, 3H), 6.29 (m, 1H), 6.96 (m, 1H), 7.66 (m, 1H), 7.80 (m, 1H), 7.99 (m, 1H), 8.18 (m, 1H), 10.80 ppm (s, 1H). ^{13}C NMR (Acetone-d$_6$, 100 MHz): $\delta = 24.2$, 32.5, 44.2, 108.8, 109.1, 122.4, 126.1, 128.6, 130.8, 133.0, 143.1, 150.6, 156.8, 173.5 ppm. HRMS (FAB−): calcd for $C_{14}H_{13}O_5S$: 293.0484; found: 293.0452.

3-(5-Pyridine-3-yl-furan-2-yl)propanoic acid (**7i**): orange-brown solid, yield: 47%. FC: silica gel, CH_2Cl_2/MeOH 95:5. ^{1}H NMR ([D$_6$]DMSO, 500 MHz): $\delta = 2.44$ (t, $J = 7.7$ Hz, 2H), 2.88 (t, $J = 7.7$ Hz, 2H), 6.24 (m, 1H), 6.97 (m, 1H), 7.41 (m, 1H), 7.98 (m, 1H), 8.43 (m, 1H), 8.80 (m, 1H), 12.25 ppm (s, 1H). ^{13}C NMR ([D$_6$]DMSO, 125 MHz): $\delta = 23.2$, 31.9, 107.8, 108.2, 123.9, 126.5, 130.1, 144.4, 147.8, 148.8, 155.6, 173.5 ppm. HRMS (EI): calcd for $C_{12}H_{11}NO_3$: 217.0739; found: 217.0717.

3-(5-Pyridine-2-yl-furan-2-yl)propanoic acid (**7j**): orange-brown solid, yield: 90%. ^{1}H NMR ([D$_6$]DMSO, 500 MHz): $\delta = 2.45$ (t, $J =$ 7.4 Hz, 2H), 2.89 (t, $J = 7.4$ Hz, 2H), 6.26 (m, 1H), 6.97 (m, 1H), 7.22 (m, 1H), 7.64 (m, 1H), 7.80 (m, 1H), 8.52 ppm (m, 1H). ^{13}C NMR ([D$_6$]DMSO, 125 MHz): $\delta = 23.9$, 33.3, 107.6, 109.6, 117.7, 121.8, 136.9, 148.6, 149.4, 151.4, 156.8, 174.9 ppm. HRMS (EI): calcd for $C_{12}H_{11}NO_3$: 217.0739; found: 217.0778.

3-(5-Phenylthiophene-2-yl)propanoic acid (**8a**): pale orange solid, yield: 17%. FC: silica gel, CH_2Cl_2/MeOH 9:1. H NMR ([D$_6$]DMSO, 500 MHz): $\delta = 2.61$ (t, $J = 7.4$ Hz, 2H), 3.03 (t, $J = 7.4$ Hz, 2H), 6.88 (m, 1H), 7.27 (m, 1H), 7.31 (m, 1H), 7.37–7.41 (m, 2H), 7.57–7.60 (m, 2H), 12.30 ppm (s, 1H). ^{13}C NMR ([D$_6$]DMSO, 125 MHz): $\delta = 25.0$, 35.3, 123.3, 125.0, 126.0, 127.2, 129.1, 133.9, 141.0, 143.3, 173.3 ppm. HRMS (EI): calcd for $C_{13}H_{12}O_2S$: 232.0558; found: 232.0565.

3-(5-(3-Methylphenyl)thiophene-2-yl)propanoic acid (**8b**): pale orange solid, yield: 60%. ^{1}H NMR ([D$_6$]DMSO, 500 MHz): $\delta = 2.32$ (s, 3H), 2.55 (t, $J = 7.4$ Hz, 2H), 3.01 (t, $J = 7.4$ Hz, 2H), 6.85 (m, 1H), 7.08 (m, 1H), 7.26 (m, 1H), 7.28 (m, 1H), 7.35–7.40 (m, 2H), 12.60 ppm (b, 1H). ^{13}C NMR ([D$_6$]DMSO, 100 MHz): $\delta = 21.0$, 25.3, 36.1, 122.2, 123.2, 125.5, 125.9, 128.0, 129.0, 133.9, 138.3, 141.1, 143.6, 174.4 ppm. HRMS (EI): calcd for $C_{14}H_{14}O_2S$: 246.0715; found: 246.0701.

3-(5-(3-Methoxyphenyl)thiophene-2-yl)propanoic acid (**8c**): orange solid, yield: 72%. FC: silica gel, CH_2Cl_2/MeOH 95:5. ^{1}H NMR ([D$_6$]DMSO, 500 MHz): $\delta = 2.61$ (t, $J = 7.3$ Hz, 2H), 3.02 (t, $J = 7.3$ Hz, 2H), 3.79 (s, 3H), 6.83–6.89 (m, 2H), 7.11 (m, 1H), 7.14 (m, 1H), 7.30 (m, 1H), 7.33 (m, 1H), 12.30 ppm (s, 1H). ^{13}C NMR ([D$_6$]DMSO, 125 MHz): $\delta = 24.8$, 35.2, 55.0, 110.3, 112.8, 117.4, 123.6, 125.9, 130.1, 135.2, 140.8, 143.3, 159.6, 173.2 ppm. HRMS (EI): calcd for $C_{14}H_{14}O_3S$: 262.0664; found: 262.0678.

3-(5-(3-(Trifluormethyl)phenyl)thiophene-2-yl)propanoic acid (**8d**): pale yellowish solid, Yield: 45%. FC: silica gel, CH_2Cl_2/MeOH 95:5. ^{1}H NMR ([D$_6$]DMSO, 500 MHz): $\delta = 2.62$ (t, $J = 7.3$ Hz, 2H), 3.05 (t, $J = 7.3$ Hz, 2H), 6.93 (m, 1H), 7.52 (m, 1H), 7.61–7.65 (m, 2H), 7.86–7.90 (m, 2H), 12.32 ppm (s, 1H). ^{13}C NMR ([D$_6$]DMSO, 125 MHz): $\delta =$ 24.9, 35.2, 121.0 (q, $J_{CF} = 3.8$ Hz), 123.6 (q, $J_{C-F} = 1.9$ Hz,), 124.0 (q, $J_{C-F} = 272.5$ Hz), 125.0, 126.4, 129.0, 129.9 (q, $J_{C-F} = 31.7$ Hz), 130.3, 134.9 (q, $J_{C-F} = 1.9$ Hz), 139.0, 144.7, 173.3 ppm. HRMS (EI): calcd for $C_{14}H_{11}F_3O_2S$: 300.0432; found: 300.0432.

3-(2-Phenythiazole-5-yl)propanoic acid (**15**): ochre solid, yield: 51%. FC: silica gel, CH_2Cl_2/MeOH 95:5. ^{1}H NMR ([D$_6$]DMSO, 400 MHz): $\delta =$ 2.62 (t, $J = 7.3$ Hz, 2H), 3.09 (t, $J = 7.3$ Hz, 2H), 7.43–7.52 (m, 3H), 7.66 (m, 1H), 7.85–7.90 ppm (m, 2H). ^{13}C NMR ([D$_6$]DMSO, 125 MHz): $\delta = 22.2$, 36.2, 125.8, 132.2, 129.8, 133.4, 139.1, 141.1, 165.4, 174.2 ppm. HRMS (EI): calcd for $C_{12}H_{11}NO_2S$: 233.0510; found: 233.0538.

3-(2-Phenylthiazole-4-yl)propanoic acid (**18**): After hydrogenation, the residue was heated to reflux for 1 h. The white residue was filtered off and dried to give compound **18** as a white solid (69%). ^{1}H NMR ([D$_6$]DMSO, 500 MHz): $\delta = 2.55$ (t, $J = 7.6$ Hz, 2H), 2.99 (t, $J = 7.6$ Hz, 2H), 7.33 (s, 1H), 7.44–7.51 (m, 3H), 7.89–7.92 ppm (m, 2H). ^{13}C NMR ([D$_6$]DMSO, 100 MHz): $\delta = 27.7$, 35.9, 114.0, 125.9, 129.2, 130.0, 133.2, 158.1, 166.1, 178.4 ppm. HRMS (EI): calcd for $C_{12}H_{11}NO_2S$: 233.0510; found: 233.0513.

5-(3-Nitrophenyl)furan-2-yl-methanol (**9**): 5-(3-Nitrophenyl)furan-2-yl carboxaldehyde (870 mg, 4.00 mmol) was dissolved in THF. $NaBH_4$ (113 mg, 3.0 mmol) was added and the mixture was stirred overnight at RT. Water was added and the reaction was stirred for 1 h, the mixture was extracted with Et_2O (×3). The combined organic layers were dried (Na_2SO_4) and evaporated resulting in a yellow solid (99%). ^{1}H NMR ($CDCl_3$, 500 MHz): $\delta = 1.80$ (s, 1H), 4.70 (s, 2H), 6.44 (m, 1H), 6.76 (m, 1H), 7.54 (m, 1H), 7.94–7.97 (m, 1H), 8.09 (m, 1H), 8.49 ppm (m, 1H).

5-(3-Nitrophenyl)thiophene-2-yl-methanol (**10**): 5-(3-Nitrophenyl) thiophene-2-yl carboxaldehyde (320 mg, 1.40 mmol) was dissolved in THF. $NaBH_4$ (38 mg, 1.0 mmol) was added and stirred overnight at RT. After adding H_2O and stirring for one hour, the mixture was extracted with Et_2O (×3). The combined organic layers were dried (Na_2SO_4) and evaporated resulting in a orange solid (83%). ^{1}H NMR ($CDCl_3$, 500 MHz) $\delta = 1.81$ (s, 1H), 4.69 (s, 2H), 6.93 (m, 1H), 7.15 (m, 1H), 7.55 (m, 1H), 7.92–8.00 (m, 1H), 8.08–8.13 (m, 1H), 8.43 ppm (m, 1H).

2-Chloromethyl-5-(3-nitrophenyl)furan: 5-(3-Nitrophenyl)furan-2-yl-methanol (**9**) (1.0 equiv) was dissolved in CH_2Cl_2. The solution was treated with $SOCl_2$ (1.2 equiv) and then stirred for 1 h. The solvent and excess $SOCl_2$ were evaporated and the resulting residue was immediately used for the following reaction without further purification or characterization.

Diethyl-2-(5-(3-nitrophenyl)furan-2-yl-methyl) malonate (**11**): Under an inert atmosphere, NaH (60% suspension in paraffin oil; 320 mg, 8.0 mmol) was suspended in dry THF and cooled in an ice bath. Diethyl malonate (1.28 g, 8.0 mmol) was added dropwise. The mixture was stirred, warming to RT until obtaining a clear solution. A solution of 2-chloromethyl-5-(3-nitrophenyl)furan (930 mg, 3.90 mmol) in dry THF was added dropwise and the mixture was stirred for 18 h. The solvent was evaporated and the residue was dissolved in Et_2O and washed with water (×3). The organic layer was dried (Na_2SO_4) and evaporated. The resulting material was sub-

 © 2009 Wiley-VCH Verlag GmbH & Co. KGaA, Weinheim

jected to flash chromatography (silica gel, isohexane/EtOAc, 4:1) to afford the product as an orange oil (54%). ^{1}H NMR (Acetone-d$_6$, 500 MHz): δ=1.21 (t, J=7.1 Hz, 6H), 3.32 (d, J=7.7 Hz, 2H), 3.88 (t, J=7.7 Hz, 1H), 4.15–4.23 (m, 4H), 6.35 (m, 1H), 7.03 (m, 1H), 7.70 (m, 1H), 8.07–8.12 (m, 2H), 8.44 ppm (m, 1H).

2-Chloromethyl-5-(3-nitrophenyl)thiophene: 5-(3-Nitrophenyl)-thiophene-2-yl-methanol (**10**) (1.0 equiv) was dissolved in CH_2Cl_2. The solution was treated with $SOCl_2$ (1.2 equiv) and then stirred for 1 h. The solvent and excess $SOCl_2$ were evaporated and the resulting residue was immediately used for the following reaction without further purification or characterization.

Diethyl-2-(5-(3-nitrophenyl)thiophene-2-yl-methyl) malonate (**12**): Under an inert atmosphere NaH (60% suspension in paraffine oil; 112 mg, 2.8 mmol) was suspended in dry THF and cooled in an ice bath. Diethyl malonate (448 mg, 2.8 mmol) was added dropwise. The mixture was stirred, warming to RT until a clear solution was obtained. A solution of 2-chloromethyl-5-(3-nitrophenyl)furan (355 mg, 1.40 mmol,) in dry THF was added dropwise and the mixture was stirred for 18 h. The solvent was evaporated and the residue was dissolved in Et_2O and washed with water (×3). The organic layer was dried (Na_2SO_4) and evaporated. The resulting material was subjected to flash silica gel chromatography (isohexane/EtOAc, 4:1) to afford the product as a yellow solid (49%). ^{1}H NMR ($CDCl_3$, 500 MHz): δ=1.23 (t, J=7.1 Hz, 6H), 3.44 (d, J=7.6 Hz, 2H), 3.69 (t, J=7.6 Hz, 1H), 4.18–4.26 (m, 4H), 6.86 (m, 1H), 7.23 (m, 1H), 7.52 (m, 1H), 7.80–7.84 (m, 1H), 8.06–8.10 (m, 1H), 8.37 ppm (m, 1H).

3-(5-(3-Nitrophenyl)furan-2-yl)propanoic acid (**7h**): Diethyl-2-(5-(3-nitrophenyl)furan-2-yl-methyl)malonate (**11**) (628 mg, 1.75 mmol) was suspended in aq HCl (6 M) and heated at reflux for 6 h. After cooling the mixture was extracted with EtOAc (×3). The combined organic layers were extracted with aq KOH (5%). The aqueous layer was then adjusted to pH 1 with aq HCl (20%). The precipitate was filtered off and washed with water to give **7h** as a yellow-orange solid (51%). ^{1}H NMR (Acetone-d$_6$, 500 MHz): δ=2.75 (t, J=7.5 Hz, 2H), 3.05 (t, J=7.5 Hz, 2H), 6.31 (m, 1H), 7.04 (m, 1H), 7.69 (m, 1H), 8.09 (m, 2H), 8.45 (m, 1H), 10.20 ppm (s, 1H). ^{13}C NMR (Acetone-d$_6$, 100 MHz): δ=24.2, 32.4, 108.9, 109.6, 118.2, 122.0, 129.7, 131.1, 133.4, 149.8, 150.8), 157.1, 173.5 ppm. HRMS (EI): calcd for $C_{13}H_{11}NO_5$: 261.0637; found: 261.0650.

3-(5-(3-Nitrophenyl)thiophene-2-yl)propanoic acid (**8h**): Diethyl-2-(5-(3-nitrophenyl)thiophene-2-yl-methyl)malonate (**12**) (249 mg, 0.66 mmol) was suspended in aq HCl (6 M) and heated at reflux for 6 h. After cooling down the mixture was extracted with EtOAc (×3). The combined organic layers were extracted with aq KOH (5%). The aqueous layer was then adjusted to pH 1 with aq HCl (20%). The precipitate was filtered off and washed with water to give **8h** as an ochre solid (62%). ^{1}H NMR (Acetone-d$_6$, 500 MHz): δ=2.73 (t, J=7.3 Hz, 2H), 3.17 (t, J=7.3 Hz, 2H), 6.97 (m, 1H), 7.50 (m, 1H), 7.69 (m, 1H), 8.03 (m, 1H), 8.11 (m, 1H), 8.38 (m, 1H), 10.70 ppm (b, 1H). ^{13}C NMR (Acetone-d$_6$, 100 MHz): δ=26.0, 35.8, 120.2, 122.4, 126.1, 127.4, 131.3, 131.0, 137.1, 140.0, 146.4, 149.8, 173.4 ppm. HRMS (EI): calcd for $C_{13}H_{11}NO_4S$: 277.0411; found: 277.0411.

5-(3-Methylphenyl)thiophene (**19b**) was prepared in the same manner as described in the procedure for the preparation of carbaldehydes by Suzuki coupling 3-methylphenylboronic acid (1.20 g, 8.80 mmol) with 2-bromothiophene to give the product after FC (isohexane/EtOAc, 9:1) as a yellow oil (790 mg, 57%). ^{1}H NMR ($CDCl_3$, 500 MHz): δ=2.39 (s, 3H), 7.07 (m, 1H), 7.10 (m, 1H), 7.25–7.28 (m, 2H), 7.30 (m, 1H), 7.40–7.44 ppm (m, 2H).

*General procedure 4: Preparation of the 4-oxobutanoic acids (**20**) via Friedel–Crafts acylation.*

The reaction was carried out under an inert atmosphere. The biaryl component and powdered succinic anhydride (1.0 equiv) were dissolved in 1,2-dichloroethane. The mixture was cooled to 0°C and $AlCl_3$ (2.2 equiv) was added. After stirring for 5 h at 0°C the reaction mixture was warmed to RT overnight. A solution of aq HCl (10%) was added and the mixture was stirred for a further 30 min. After extracting with EtOAc, the combined organic layers were extracted with aq KOH (5%). This layer was adjusted to pH 1 with aq HCl (10%). The resulting precipitation was filtered off, washed with water and dried.

4-Oxo-4-(5-phenylthiophen-2-yl)butanoic acid (**20a**): yellowish solid, yield: 86%. ^{1}H NMR ([D$_6$]DMSO, 500 MHz): δ=2.59 (t, J=6.6 Hz, 2H), 3.21 (t, J=6.6 Hz, 2H), 7.42 (m, 1H), 7.47 (m, 2H), 7.66 (m, 1H), 7.77–7.80 (m, 2H), 8.01 (m, 1H), 12.20 ppm (s, 1H). ^{13}C NMR ([D$_6$]DMSO, 125 MHz) δ=27.1, 32.4, 124.3, 125.3, 128.4, 128.6, 131.9, 133.7, 141.3, 150.3, 172.9, 190.7 ppm. HRMS (EI): calcd for $C_{14}H_{12}O_3S$: 260.0507; found: 260.0554.

4-Oxo-4-(5-(3-methylphenyl)thiophene-2-yl)butanoic acid (**20b**): dark orange solid, yield: 50%. ^{1}H NMR ([D$_6$]DMSO, 500 MHz): δ=2.36 (s, 3H), 2.58 (t, J=5.7 Hz, 2H), 3.20 (t, J=5.7 Hz, 2H), 7.24 (m, 1H), 7.35 (m, 1H), 7.56 (m, 1H), 7.60 (s, 1H), 7.63 (m, 1H), 7.98 (m, 1H), 12.20 (s, 1H). ^{13}C NMR ([D$_6$]DMSO, 100 MHz): δ=20.9, 27.9, 33.1, 123.2, 124.9, 126.5, 129.2, 129.9 (Aryl-CH), 132.6 (qC-1′′), 134.4, 138.7, 141.9, 151.3, 173.7, 191.5 ppm. HRMS (EI): calcd for $C_{15}H_{14}O_3S$: 274.0664; found: 274.0686.

*General procedure 5: Preparation of butanoic acids (**21**) via Wolff–Kishner reduction.*

To a stirred solution of the 4-oxo-butanoic acid (1.0 equiv) in diethylene glycol (2 mL mmol^{-1} oxobutanoic acid), $NH_2NH_2{\cdot}H_2O$ (4.0 equiv) and KOH (4.0 equiv) were added. The mixture was heated to a temperature of 180°C. After cooling, the mixture was diluted with H_2O (10 mL mmol^{-1} oxobutanoic acid). The mixture was extracted once with EtOAc and adjusted to pH 1 with aq HCl (10%) and again extracted with EtOAc (×3). The combined organic layers were extracted with aq KOH (5%). The aqueous layer was adjusted to pH 1. The precipitation was filtered off and washed with water to give the butanoic acid derivative.

4-(5-Phenylthiophene-2-yl)butanoic acid (**21a**): orange solid, yield: 53%. ^{1}H NMR ($CDCl_3$, 500 MHz): δ=2.04 (tt, J_1=J_2=7.5 Hz, 2H), 2.45 (t, J=7.5 Hz, 2H), 2.90 (t, J=7.5 Hz, 2H), 6.77 (m, 1H), 7.12 (m, 1H), 7.22–7.27 (m, 1H), 7.32–7.38 (m, 2H), 7.53–7.57 ppm (m, 2H). HRMS (EI): calcd for $C_{14}H_{14}O_2S$: 246.0715; found: 246.0749.

4-(5-(3-Methylphenyl)thiophene-2-yl)butanoic acid (**21b**): orange solid, yield: 47%. ^{1}H NMR ([D$_4$]MeOH, 400 MHz): δ=1.97 (tt, J_1=J_2=7.5 Hz, 2H), 2.35 (s, 3H), 2.37 (t, J=7.5 Hz, 2H), 2.86 (t, J=7.5 Hz, 2H), 6.78 (m, 1H), 7.06 (m, 1H), 7.16 (m, 1H), 7.22 (m, 1H), 7.35 (m, 1H), 7.39 ppm (s, 1H). ^{13}C NMR ([D$_4$]MeOH, 125 MHz): δ=21.5, 28.1, 30.3, 34.0, 123.6, 123.8, 126.8, 127.0, 128.9, 129.8, 136.0, 139.7, 143.5, 145.1, 177.1 ppm. HRMS (EI): calcd for $C_{15}H_{16}O_2S$: 260.0871; found: 260.0872.

Acknowledgements

We thank Dr. Alberto Podjarny, IGBMC, Illkirch (France) for providing us with the expression clone of human ALR2. The bilateral financial support of CNRS and DFG under the CERC3 program

 © 2009 Wiley-VCH Verlag GmbH & Co. KGaA, Weinheim

(KL1204/3, KL1204/4), as well as the Graduiertenkolleg ''Protein function at the atomic level'', is gratefully acknowledged.

Keywords: drug design · lead optimization · structure–activity relationships · aldose reductase · inhibitors · diabetes

[1] C. L. Kaul, P. Ramarao, *Methods Find. Exp. Clin. Pharmacol.* **2001**, *23*, 465–475.
[2] A. Lindholm, *Best Pract. Res. Clin. Gastroenterol.* **2002**, *16*, 475–492.
[3] The Diabetes Control and Complications Trial Research Group, *N. Engl. J. Med.* **1993**, *329*, 977–986.
[4] UK Prospective Diabetes Study (UKPDS) Group, *Lancet* **1998**, *352*, 837–853.
[5] American Diabetes Association, *Diabetes Care* **2003**, *26 Suppl 1*, S33–50.
[6] K. L. Bate, G. Jerums, *Med. J. Aust.* **2003**, *179*, 498–503.
[7] P. Valensi, C. Le Devehat, J.-L. Richard, C. Farez, T. Khodabandehlou, R. A. Rosenbloom, C. LeFante, *J. Diabetes Complications* **2005**, *19*, 247–253.
[8] V. M. Altan, *Curr. Med. Chem.* **2003**, *10*, 1317.
[9] R. G. Gonzalez, P. Barnett, H.-M. Cheng, J. L. T. Chylack, *Exp. Eye Res.* **1984**, *39*, 553.
[10] C. Yabe-Nishimura, *Pharmacol. Rev.* **1998**, *50*, 21–33.
[11] L. Costantino, G. Rastelli, P. Vianello, G. Cignarella, D. Barlocco, *Med. Res. Rev.* **1999**, *19*, 3–23.
[12] D. A. Greene, S. A. Lattimer, A. A. Sima, *N. Engl. J. Med.* **1987**, *316*, 599–606.
[13] D. Giugliano, A. Ceriello, G. Paolisso, *Metabolism* **1995**, *44*, 363–368.
[14] M. Brownlee, *Annu. Rev. Med.* **1995**, *46*, 223–234.
[15] Anonymous, *Drugs R&D* **2002**, *3*, 235–237.
[16] S. Suzen, E. Buyukbingol, *Curr. Med. Chem.* **2003**, *10*, 1329–1352.
[17] S. S. Chung, S. K. Chung, *Curr Drug Targets* **2005**, *6*, 475–486.
[18] C. Nishimura, Y. Matsuura, Y. Kokai, T. Akera, D. Carper, N. Morjana, C. Lyons, T. G. Flynn, *J. Biol. Chem.* **1990**, *265*, 9788–9792.
[19] C. A. Sotriffer, O. Kramer, G. Klebe, *Proteins Struct. Funct. Bioinf. Proteins* **2004**, *56*, 52–66.
[20] O. El-Kabbani, C. Darmanin, T. R. Schneider, I. Hazemann, F. Ruiz, M. Oka, A. Joachimiak, C. Schulze-Briese, T. Tomizaki, A. Mitschler, A. Podjarny, *Proteins Struct. Funct. Bioinf. Proteins* **2004**, *55*, 805–813.
[21] O. El-Kabbani, D. K. Wilson, M. Petrash, F. A. Quiocho, *Mol. Vision* **1998**, *4*, 19.
[22] M. Oka, Y. Matsumoto, S. Sugiyama, N. Tsuruta, M. Matsushima, *J. Med. Chem.* **2000**, *43*, 2479–2483.
[23] H. Steuber, M. Zentgraf, A. Podjarny, A. Heine, G. Klebe, *J. Mol. Biol.* **2006**, *356*, 45–56.
[24] E. I. Howard, R. Sanishvili, R. E. Cachau, A. Mitschler, B. Chevrier, P. Barth, V. Lamour, M. Van Zandt, E. Sibley, C. Bon, D. Moras, T. R. Schneider, A. Joachimiak, A. Podjarny, *Proteins Struct. Funct. Bioinf. Proteins* **2004**, *55*, 792–804.
[25] O. Kraemer, I. Hazemann, A. D. Podjarny, G. Klebe, *Proteins Struct. Funct. Bioinf. Proteins* **2004**, *55*, 814.
[26] H. Steuber, A. Heine, G. Klebe, *J. Mol. Biol.* **2007**, *368*, 618–638.
[27] GraFit Version 4.0, R. J. Leatherbarrow, Erithacus Software Ltd., Staines (UK), **1998**.
[28] Z. Otwinowski, W. Minor, *Methods Enzymol.* **1997**, *276*, 307–326.
[29] A. T. Brünger, P. D. Adams, G. M. Clore, W. L. DeLano, P. Gros, R. W. Grosse-Kunstleve, J. S. Jiang, J. Kuszewski, M. Nilges, N. S. Pannu, R. J. Read, L. M. Rice, T. Simonson, G. L. Warren, *Acta Crystallogr., Sect. D: Biol. Crystallogr.* **1998**, *54*, 905–921.
[30] G. M. Sheldrick, T. R. Schneider, *Methods Enzymol.* **1997**, *277*, 319–343.
[31] T. A. Jones, J. Y. Zou, S. W. Cowan, M. Kjeldgaard, *Acta Crystallogr., Sect. A: Cryst. Phys., Diffr., Theor. Gen. Crystallogr.* **1991**, *47*, 110–119.
[32] R. A. Laskowski, M. W. MacArthur, D. S. Moss, J. M. Thornton, *J. Appl. Crystallogr.* **1993**, *26*, 283–291.
[33] PyMOL Molecular Graphics System (http://www.pymol.org), W. L. DeLano, DeLano Scientific LLC, Palo Alto (USA), **2002**.
[34] J. C. Bussolari, D. C. Rehborn, *Org. Lett.* **1999**, *1*, 965–967.
[35] A. Silberg, *Chem. Ber.* **1961**, *94*, 2887–2894.
[36] A. Silberg, *Chem. Ber.* **1964**, *97*, 1684–1687.
[37] A. Mitsch, P. Wißner, K. Silber, P. Haebel, I. Sattler, G. Klebe, M. Schlitzer, *Bioorg. Med. Chem.* **2004**, *12*, 4585–4600.
[38] A. Mitsch, M. Altenkämper, I. Sattler, M. Schlitzer, *Arch. Pharm. Chem. Life Sci.* **2005**, *338*, 9–17.

Received: November 27, 2008
Revised: February 9, 2009
Published online on ■■ ■■, 2009

 © 2009 Wiley-VCH Verlag GmbH & Co. KGaA, Weinheim

M. Eisenmann, H. Steuber, M. Zentgraf, M. Altenkämper, R. Ortmann, J. Perruchon, G. Klebe, M. Schlitzer**

■■ – ■■

Structure-Based Optimization of Aldose Reductase Inhibitors Originating from Virtual Screening

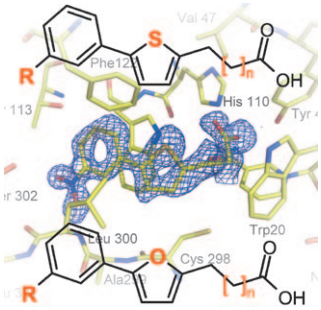

Virtual screening discovered two prospective hits as potential leads for aldose reductase inhibition. Based on their crystal structures with the enzyme, a systematic optimization has been performed to reveal a first structure–activity relationship. A central thiophen moiety and a terminal nitro group exhibit the best binding properties.

 © 2009 Wiley-VCH Verlag GmbH & Co. KGaA, Weinheim